Department of Physics
Ludwig-Maximilians-University Munich

Master Thesis in Physics
submitted by

Robin Eberhard
born in Aalen, Germany

handed in on

October 16, 2020

Spin Selective Imaging of Ground State Potassium Atoms

This Bachelor Thesis has been carried out by Robin Eberhard at the
Physics Institute in **Munich**
under the supervision of
Prof. Dr. Christian Gross

Spin Selective Imaging of Ground State Potassium Atoms

Robin Eberhard

Abstract Abstract

Zusammenfassung Abstract

Contents

1 Introduction

2 Motivation

3 Chopping

Better headline

Optical tweezers are a fundamental tool in the experiment allowing to have full control over the distribution of potassium atoms. To maintain control over long times, heating of atoms needs to be compensated. For potassium atoms which are cooled on the D1 line, the excited state is strongly anti-trapped, making it impossible to trap atoms that haven't decayed back to the ground state, while simultaneously cooling them. For this reason, cooling and trapping beams alternate out of phase, which can be done on a frequency scale up to the lifetime of the $^2P_{1/2}$ state. For reference, the cooling scheme for ^{39}K is discussed in [1].

So far, alternating between the two laser beams, called chopping, was achieved using an acousto-optical modulator (AOM), a device, that can deflect a laser beam based on an input sound wave and thus acting as a fast flip-mirror. This effect is limited by the speed of sound in the medium and results in a chopping frequency of 1.4 MHz, governed by the AOM with the slowest rise time, which can be seen in Figure 3. By increasing the chopping frequency, the atoms will heat less during each trapping cycle, therefore new ways of alternating the beams are sought out. In the following is discussed an electro-optical modulator (EOM), which is not limited by sound waves. The modulator is governed by the electro-optical effect, which makes it possible to change the refractive index based on an applied electric field, therefore only limiting it by the electronics that generate the field.

acronyms? MOT, SLM

The devices tested in this thesis are both capable of switching on nanosecond scales, improving the current chopping rate by three orders of magnitude. The theory behind the linear electro-optical effect is discussed after a short recourse on polarization of electromagnetic waves. Lastly, experimental evaluations for two EOMs are presented and discussed.

3.1 Theory on Polarization

Amongst frequency and amplitude, there is another parameter that can generally be affected in monochromatic electromagnetic waves, which is the polarization. It is the orien-

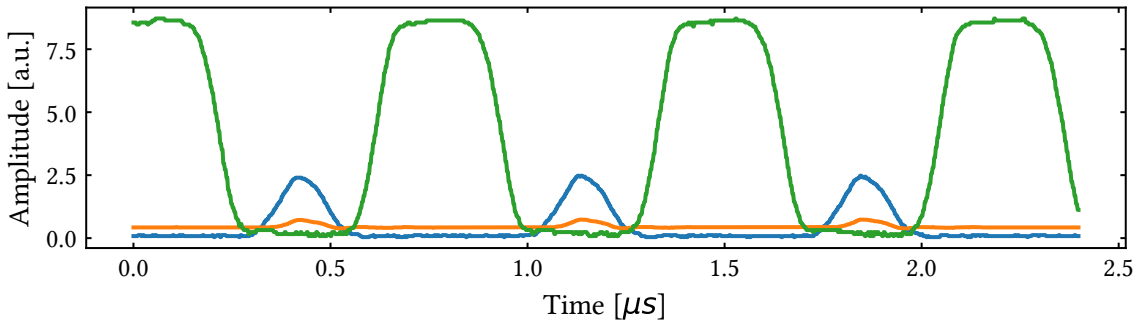

Figure 3.1: Chopping in the experiment. Laser beams alternate between each other, with blue being the MOT cooler, orange the MOT repumper and green the SLM tweezer. The amplitude of the MOT beams is limited due to the risetime of the AOMs.

Reviewers: I only discuss transverse polarization, should I keep it this way or do I make a comment about longitudinal polarization?

tation of the wave in space, transverse to the direction of movement. In general, a wave travelling along the z-axis can be oriented somewhere in the x-y plane. Therefore, writing the electric field component of the light in this basis takes the following form:

$$\mathbf{E}(\mathbf{x},t) = E_x cos\left(kx - wt + \phi_x\right)\mathbf{e_x} + E_y cos\left(ky - wt + \phi_y\right)\mathbf{e_y}. \tag{3.1}$$

Here, k and w refer to the wave number and frequency respectively. Depending on the amplitudes E_x and E_y and the phases ϕ_x and ϕ_y, the wave can be in different polarization states. If it is not possible to write the wave in this basis, the light is unpolarized. Otherwise, it is **linear**, when either one of the amplitudes E_x or E_y is zero or when the phase difference $\Delta\phi = \phi_x - \phi_y$ evaluates to 0 or π. It is **circular**, when the phase difference $\Delta\phi = \pm\pi/2$ and the amplitudes are the same, $E_x = E_y$. In any other case, the wave is **elliptically** polarized.

From this point, we can see how to create a device that modifies the polarization. We can do this by retarding one axis stronger than another. Given a material with two refractive indices n_x and n_y along the axes x and y, we then get the phase shifts:

$$\phi_x(z) = k_0 n_x z \tag{3.2}$$

$$\phi_y(z) = k_0 n_y z \tag{3.3}$$

where k_0 is the free space wave vector of the light. Then a device that retards the phase difference $\Delta\phi$ by $\pi/2$, which is a quarter of the wavelength, can change linearly polarized light to circularly polarized light (or vice-versa) and is therefore called a $\lambda/4$ waveplate. Similarily, if the phase difference is changed by $\Delta\phi = \pi$, or a half wavelength, then we can turn linear polarization around a given axis or change the orientation of circularly polarized light. This is then called a $\lambda/2$ waveplate.

3.2 Electro-optical modulators

Light travelling through a material generally has a speed smaller than the speed of light. This property of the material is the refractive index and is the ratio of the speed of light in the material to the speed of light in vacuum. Materials can change their refractive index by being exposed to an electric field, which in EOMs is generally a crystal connected to two electrodes. There are two prominent electro-optical effects that need to be distinguished. If the refractive index changes linearly with the electric field, the effect is called Pockels effect and the EOM is called a pockels cell. However if it changes with the square of the electric field, the effect is called Kerr effect. For this thesis, two Pockels cells were studied and therefore we will only discuss the pockels effect.

Reviewers: Philip proposed to mention the dispersion relation, but I'm not sure if it's relevant and how to work it in

3.2.1 Pockels effect

Following the argumentation from the book Fundamentals of Photonics [2], the pockels effect can be found by evaluating the refractive index with respect to the electric field applied to the modulator. Writing this as $n(E)$ and applying a taylor expansion, we get the following expression:

$$n(E) = n_0 + \frac{dn}{dE}E + \mathcal{O}(E^2) \tag{3.4}$$

To the reviewers: the book does the derivation using the electric impermeability, but maybe it makes sense

The pockels effect is the linear dependence of the refractive index to the electric field, therefore higher orders are neglected. The prefactor can also be found by the change of electric impermeability $\Delta\eta$, which is the ability of a material to be penetrated by an electromagnetic field. From

$$\eta = \frac{1}{n_0^2}, \tag{3.5}$$

we get

$$\Delta\eta = \frac{d\eta}{dn_0}\Delta n = -\frac{2}{n_0^3}\frac{dn}{dE}E = \mathfrak{r}E. \tag{3.6}$$

This results in the quantity $\mathfrak{r} = -\frac{2}{n_0^3}\frac{dn}{dE}$, which is called the Pockels coefficient given in units of $\mathrm{m\,V^{-1}}$. It can be measured by evaluating the refractive index of the material:

$$n(E) = n_0 - \frac{1}{2}\mathfrak{r}n_0^3E. \tag{3.7}$$

The pockels cells in this application act as dynamic wave retarders, therefore with the results from section 3.1, we can tune the phase difference $\Delta\phi = \phi_x - \phi_y$ along the axes x and y by applying an electric field.

We can see the effect on the phase difference by combining 3.1 and 3.2.1:

$$\begin{aligned}
\phi &= k_0Ln && (3.8)\\
&= k_0Ln_0 - \frac{k_0}{2}L\mathfrak{r}n_0^3E && (3.9)\\
&= \phi_0 - \frac{k_0}{2}L\mathfrak{r}n_0^3E && (3.10)\\
&= \phi_0 - \frac{\pi}{\lambda_0}L\mathfrak{r}n_0^3E && (3.11)
\end{aligned}$$

where the relation $k_0 = 2\pi/\lambda_0$ of the wave number was used.

It is now instructive to calculate the phase difference, which gives information about the change in polarization. The relations for the refractive indices in the two axis basis are labeled as:

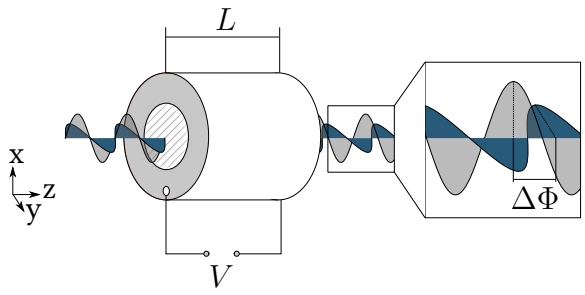

Figure 3.2: Schematic view of light passing through an EOM of length L. The electrodes are positioned on the front and back side of the modulator, the same faces the light enters and exits. The light exiting the EOM has a relative phase shift $\Delta\Phi$ depending on the change of refractive index due to the applied voltage V.

$$n_x(E) = n_{0,x} - \frac{1}{2}\mathfrak{r}_x n_{0,x}^3 E \tag{3.12}$$

$$n_y(E) = n_{0,y} - \frac{1}{2}\mathfrak{r}_y n_{0,y}^3 E \tag{3.13}$$

and then the phase difference becomes:

$$\Delta\phi = \phi_{0,x} - \phi_{0,y} - \frac{\pi}{\lambda_0} EL\left(\mathfrak{r}_x n_x^3 - \mathfrak{r}_y n_y^3\right) \tag{3.14}$$

$$\Delta\phi = \Delta\phi_0 - \frac{\pi}{\lambda_0} EL\left(\mathfrak{r}_x n_x^3 - \mathfrak{r}_y n_y^3\right). \tag{3.15}$$

The electric field is generated by applying a voltage V to two electrodes that are separated by a distance d and therefore $E = V/d$. We can then define a half-wave voltage V_π:

$$V_\pi = \frac{d}{L}\frac{\lambda_0}{\mathfrak{r}_x n_x^3 - \mathfrak{r}_y n_y^3}. \tag{3.16}$$

Thus, the phase difference can be rewritten as:

$$\Delta\phi = \Delta\phi_0 - \pi\frac{V}{V_\pi}. \tag{3.17}$$

With this it is clear, that applying the voltage V_π, the pockels cell will act as a lambda-half waveplate. A visual represantation of the modulator and the light passing through it is given in Figure 3.2.

3.2.2 Driving a pockels cell

Rise and fall times of pockels cells can go as low as nanoseconds. To make use of this speed, one has to deploy clever ways to drive the voltages, especially when these potentials are in the kilovolt-regime. For the two Pockels cells discussed in this thesis, specialized drivers by BME-Bergmann were used.

Schematically, the driver is divided into four inputs that are controlled from the user: ON A, ON B, OFF A and OFF B. These inputs control switches on either side of the pockels cell, so A controls one electrode and B the other. Most importantly, the ON X and OFF X (X referring to either A or B) switches work exclusively, so sending a high to ON X will also send a low to OFF X and vice-versa. It is then possible to apply either a positive high voltage or a negative high voltage, depending on the state of the switches. For full identification of the circuit, which is given in Figure 3.3, the side containing the positive voltage information is called high side and similarily the side containing the negative voltage information is called low side.

A requirement for our experiment is to have the EOMs work consistently. This means it is preferrable to only apply one type of voltage, because it can not be guaranteed that applying the same voltage with different polarity results in the same shift polarization. Most notably, the linearly polarized light has to be perfectly aligned on the axis of the EOM to rotate it 90° in either direction. This is in general unrealistic, not only due to human error, but also because the polarization may drift with time.

This means, only positive voltages will be applied, which results in the timing diagrams in Figure 3.5.

3.2.3 Evaluation of Leysop Pockels cells

The following pockels cells from Leysop Ltd. were chosen with the application in mind of switching light on the nanoseond scale on and off. Pockels cells can fulfill this requirement by exploiting the fact that linearly polarized light can be filtered out. This is best achieved by placing a polarizing beam splitter (PBS) directly after the modulator as seen in Figure 3.2.3. This way, the setup can be configured such that applying no voltage means light passes

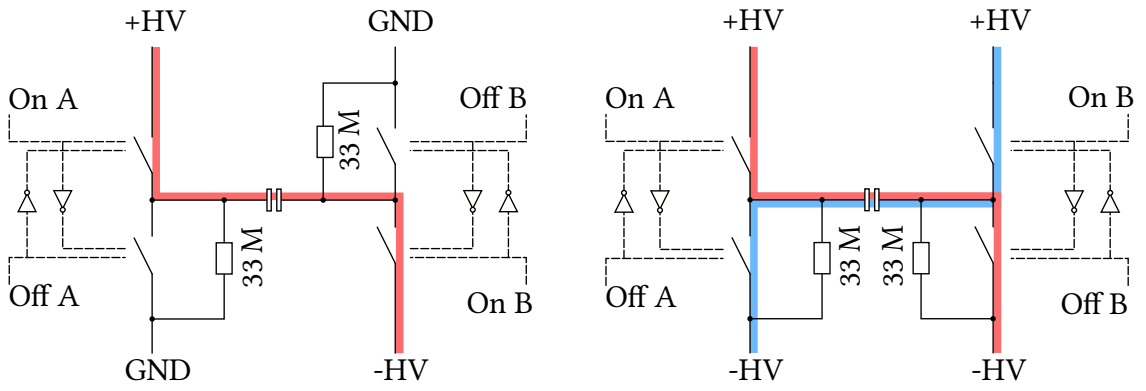

Figure 3.3: Schematic of the high voltage switches used inside the bpp-type (left) and dpp-type (right) pockels cell driver from BME Bergmann. Not-Gates on both A and B sides ensure that there is always a potential over the pockels cell. The blue and red paths indicate the connection to apply a positive and negative voltage over the pockels cell respectively.

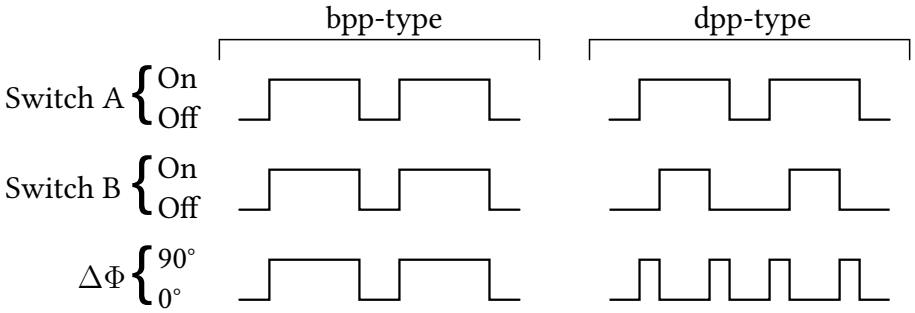

Figure 3.4: Timing diagrams for the pockels cell drivers to turn the polarization of the EOM 90°. To get a positive high voltage from the bpp-type driver, the A and B side ON/OFF switches are flipped simultaneously. The dpp-type driver is more flexible, since it also allows negative voltages. The timings displayed here are an example to only apply positive voltages across the pockels cell.

through the beam splitter, while applying V_π means the light gets reflected 90° off the beam splitter. Two pockels cells were characterized by placing a photodiode on one end of the beam splitter. The EOMs are labeled by the material of their nonlinear crystal, rubidium tanyl phosphate (RTP) and β-bariumborate (BBO). Their characteristics are summarized in table 4.3.2.

Example traces for the RTP and BBO are given in Figure 3.2.3. The peak at the start of the switch is an artifact of the photodiode. Moreover, the rise and fall times could not be resolved due to the limitations of the photodiode, a home-built model with a bandwidth of roughly 22 MHz. However, Bergmann BME lists rise and fall times of various pockels cells [3], including the ones tested here.

Stress on the crystal causes the amplitude of the laser on the output of the EOM to be

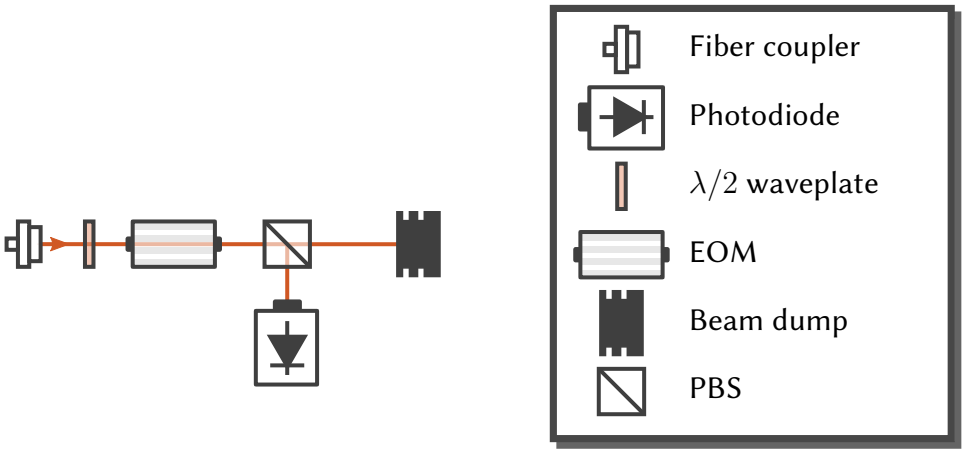

Figure 3.5: The efficiency of the EOMs were evaluated by setting the polarization of the incoming light either horizontal or vertical using the waveplate. The pockels cell will then periodically turn the polarization 90°, which can be seen by measuring the voltage on the photodiode.

inconsistent when driving the pockels cell for long times (~1 s) and high repetition rates (~MHz). This effect can be reduced by alternating the voltage applied to the crystal, which results in Figure 3.2.3, however the effect can only be seen on the RTP crystal and not on the BBO. With this information, it is clear that the RTP crystal should be driven with frequencies up to 1.2 MHz or in the range 1.5 to 1.7 MHz. The amplitude was extracted from the traces by fitting a fourier series.

In order to measure the extinction ratio, the repetition rate is set to 100 kHz, where the amplitude is consistent. Measuring first the dark current of the photodiode and then taking the signal on the output of the beam splitter results in the extinction ratio found in Figure 3.2.3.

think about the goodness of the fit

	RTP	BBO
Aperture (crystal dimensions)	3 mm	3 mm
Total crystal length (2 crystals)	30 mm	50 mm
Approximate half wave voltage (1064nm)	1.0 kV	2.8 kV
Peak damage threshold (1064nm, 1ns pulse)	$> 1\,\mathrm{GW\,cm^{-2}}$	$> 1\,\mathrm{GW\,cm^{-2}}$
Insertion loss	$< 2\,\%$	$< 1.5\,\%$

Table 3.1: Characteristics of the two pockels cells with their respective non-linear crystal materials being RTP and BBO. The aperture, damage threshold and insertion loss are given for future reference.

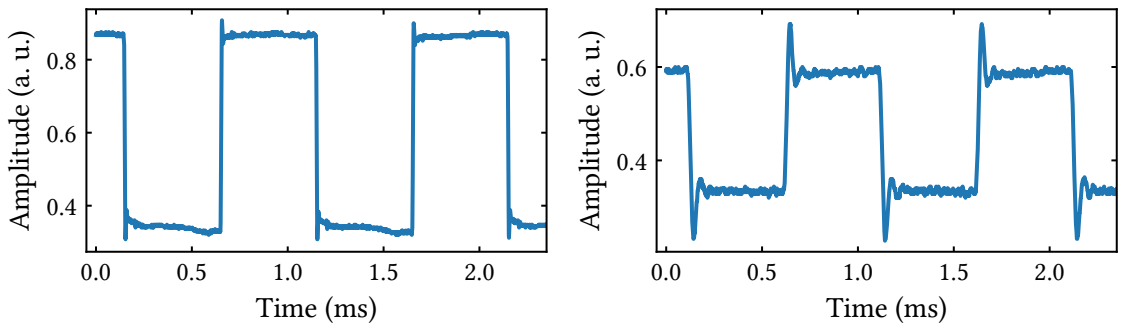

Figure 3.6: Example traces of light passing through an EOM and filtered using a polarizing beam splitter. The materials used are RTP (left) and BBO (right). The absolute value of the amplitude depends on the input power of the laser and was different for both measurements.

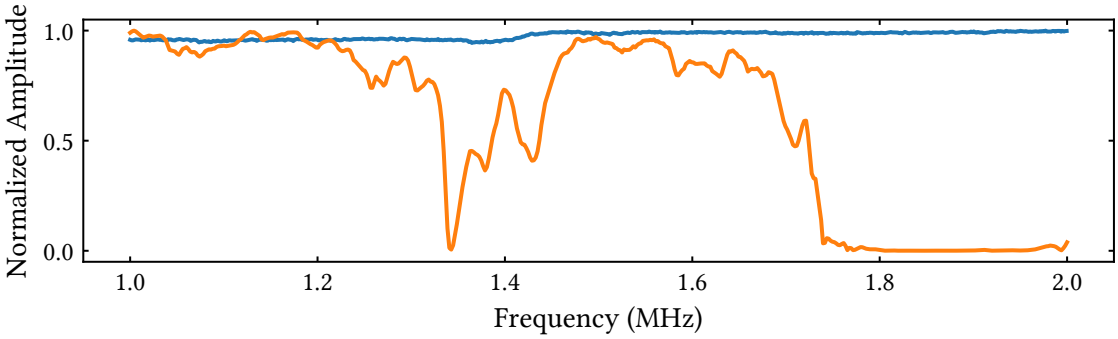

Figure 3.7: Shown is the amplitude of a laser whose polarization was rotated by a pockels cell and then filtered using a polarizing beam splitter. The frequency is the repetition rate of the voltage placed into the EOM. The two materials are RTP (orange) BBO (blue). The curves are normalized to their maximum value.

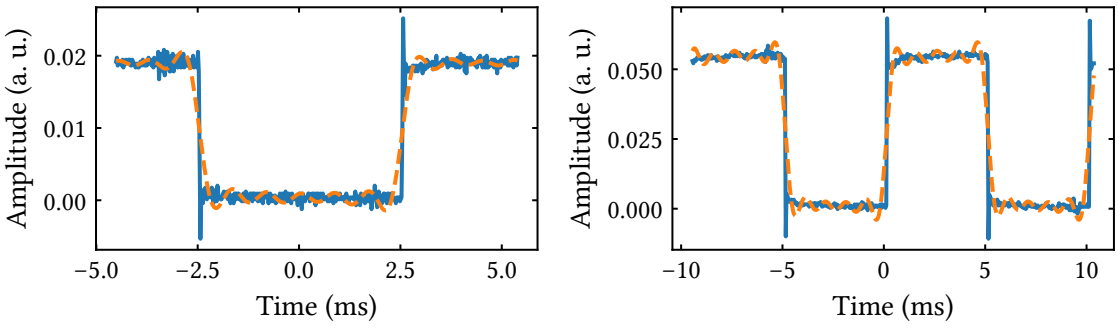

Figure 3.8: Measurements of extinction ratio for RTP (left) and BBO (right). The dashed lines indicate the fourier series fit in order to find the high and low level of the signal. The results are $> 108 : 1$ for RTP and $> 129 : 1$ for BBO.

4 Sorting of atoms

Tweezer arrays are especially suitable to study interactions between atoms, as arbitrary patterns can be set on a run-by-run basis. In order to load atoms into the tweezers, an ultracold atomic gas of ^{39}K is cooled in a grey molasses setup, before the tweezer beams are overlapped onto the gas [1]. Each trap then has equal probability of containing either even or odd numbers of atoms. However, due to light-assisted collision [4], pairs of bosons are heated out of the trap and lost, leaving only those traps occupied, which originally had an uneven number of atoms. This results in holes in the pattern, which makes it difficult to study interactions and requires a lot of effort in post-selection.

Consequently, it has become customary to rearrange the atoms of the system [5, 6], which is possible by using optical tweezers. Their dynamic nature allows repositioning of laser beams along arbitrary trajectories. By doing so adiabatically, atoms are moved along pre-calculated paths to fill gaps of the pattern. In the following is discussed the sorting of atoms by using acousto-optical deflectors (AODs) as the device of choice for programmatically deflecting a laser beam. Using this device, the beam can be split up, generating tweezers, and also make the beams move along paths to rearrange the atoms into the new pattern.

4.1 Acousto-optically deflected tweezers

Being able to quickly change the position of a laser beam is the most fundamental prerequisite of sorting atoms. The process has to happen on short timescales compared to the lifetime of atoms and with high accuracy. As such, it can't be accomplished using mechanical mirrors. However, light passing through a crystal can deflect off sound waves travelling transverse to the light direction through the medium. This is achieved using AODs and is discussed in the following.

4.1.1 Acousto-optical effect

The action that describes optical waves deflecting off sound waves is called the acousto-optical effect. It works similar to the Pockels effect from Section 3.2.1, however in this case, the medium is mechanically modulated using sound. Here, planar acoustic waves travelling through a crystal modify the refractive index [2], such that it varies with time:

$$n(x,t) = n - \Delta n_0 \cos(\Omega t - qx). \tag{4.1}$$

Using this relation, the next step is to calculate the deflection angle off the medium. In the following, a short summary is given for the steps in [2]. The medium is broken up into slices, off which the optical wave partly reflects. Each slice has a partial reflectance amplitude Δr, depending on the refractive index n and the angle of the incident optical beam with respect to the medium. The total reflectance amplitude r can then be found by integrating over all slices and will carry over the dependence on the angle. By maximizing this relation, it is then found, that the angle resulting in the maximum reflectance amplitude is given by the Bragg condition:

$$\sin\theta = \frac{\lambda_l}{2\lambda_s}, \tag{4.2}$$

where λ_l and λ_s refer to the wavelength of the light and sound waves respectively.

The maximum of the reflectance amplitude with respect to the angle is very sharp, such that in general, we can say that only if the angle between the wave vectors of the optical wave $\mathbf{k}_l$ and the sound wave $\mathbf{k}_s$ matches the Bragg condition will there be a deflected beam. Thus, another way to arrive at the Bragg condition is by finding the trigonomic relation in Figure 4.1. Using

$$|\mathbf{k}_l| = \left|\mathbf{k}_{l,r}\right| = \frac{2\pi}{\lambda_l} \tag{4.3}$$

$$|\mathbf{k}_s| = \frac{2\pi}{\lambda_s}, \tag{4.4}$$

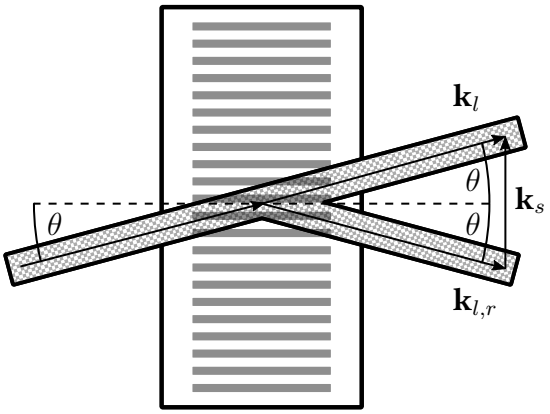

Figure 4.1: Schematic operation of an AOD. Light waves travelling in direction $\mathbf{k}_l$ are deflected off the sound waves with direction $\mathbf{k}_s$, resulting in a reflected beam $\mathbf{k}_{l,r}$. The deflection is successful, if the Bragg condition is met, which can be calculated via the vector relation $\mathbf{k}_{l,r} = \mathbf{k}_l + \mathbf{k}_s$.

it follows directly, that

$$\sin\theta = \frac{|\mathbf{k}_s|/2}{|\mathbf{k}_{l,r}|} = \frac{\lambda_l}{2\lambda_s}. \tag{4.5}$$

Using the acousto-optical effect in order to modify tweezer positions, it is necessary to break the dependence of the angle between incoming optical wave and acoustic wave, while keeping the dependence on the angle of the outgoing light. This is achieved by now modelling the sound wave as a gaussian distribution of planar waves. As such, there are waves travelling radially outwards from the origin of the sound. As a consequence of this, it will always be possible to fulfill the Bragg condition, no matter how the light enters the medium.

In Figure 4.3, an optical beam enters a medium straight and exits on a diffracted angle $\pm\theta$, given by the Bragg condition. Using again the trigonometric relations from Equation 4.5, the fact that there are acoustic waves travelling in opposing directions needs to be taken into account. In the approximation where the angle is small, the Bragg condition then simplifies to:

$$\sin\theta_\pm = \pm\frac{\lambda_l}{\lambda_s} \tag{4.6}$$

or even simpler:

$$\theta_\pm \approx \pm\frac{\lambda_l}{\lambda_s} \tag{4.7}$$

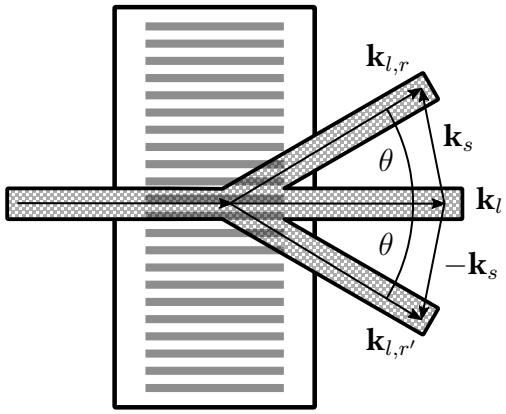

Figure 4.2: Schematic operation of an AOD. Light waves travelling in direction $\mathbf{k}_l$ are deflected off the sound waves with wave vector $\mathbf{k}_s$, resulting in a reflected beam $\mathbf{k}_{l,r}$. The deflection is successful, if the Bragg condition is met, which can be calculated via the vector relation $\mathbf{k}_{l,r} = \mathbf{k}_l + \mathbf{k}_s$.

4.1.2 Preparation of the tweezers beams

table

The deflectors used in the experiment are manufactured from Pegasus Optics and their characteristics are given in Table ??. The AODs are provided with RF-frequencies using SMA-cables. In order to deflect in two dimensions, two deflectors are placed in series, which are turned by 90° with respect to each other. This way, the first order on the first AOD will extend e.g. into the x-axis, while the first order of the second AOD will then extend along the y-axis. Together, exiting the deflectors will be a 2x2 grid of laser beams, which can be seen in Figure 4.1.2. These are the $(x = 0, y = 0)$, $(1, 0)$, $(0, 1)$ and $(1, 1)$ orders, however, only the $(1, 1)$ order will be used, as this is the one that is deflected based on the sound wave placed into the AOD.

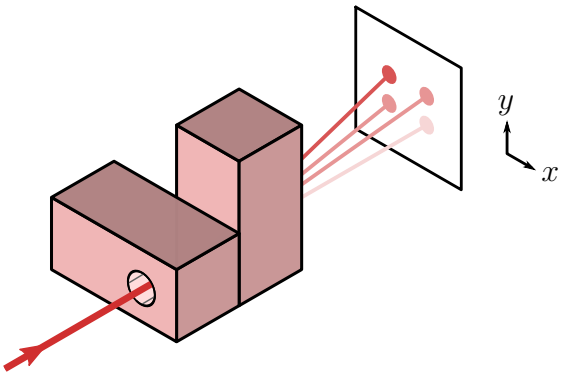

Figure 4.3: Light passing through two AODs is deflected into a 2-dimensional grid. The colors refer to the optimized power going into the respective order, from lightest color being lowest power to darkest color being highest power. This way, the least amount of power goes into the (0,0) order and most into the (1,1) order.

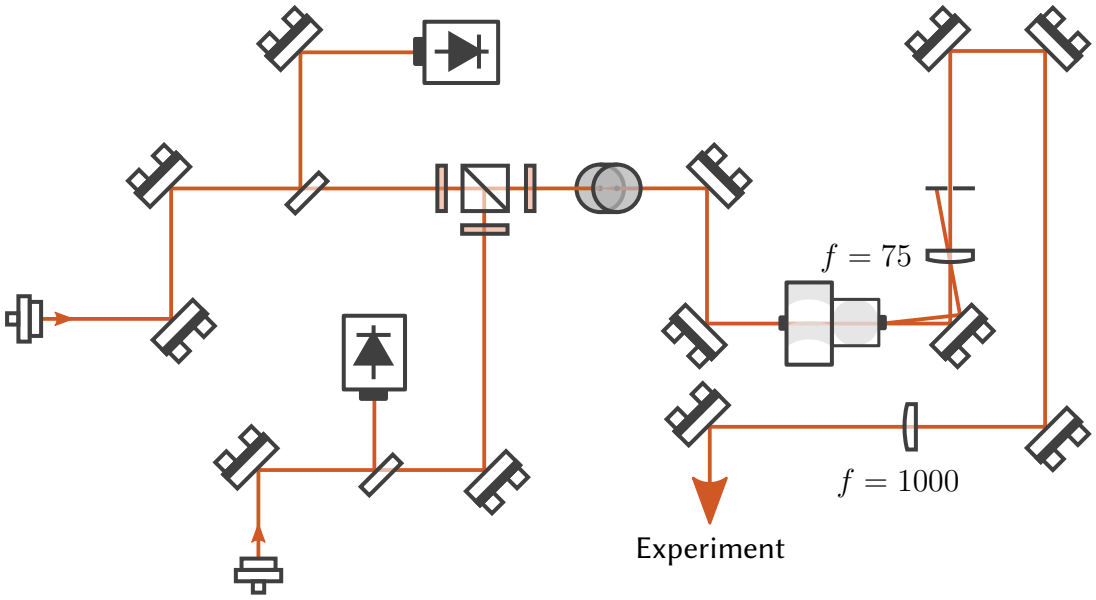

Figure 4.4: Beam path to generate acousto-optically deflected tweezers. Two beams used for sorting and spin-resolved imaging are combined using a PBS. They pass the AOD after which the beam is shaped to match the objective into the experimental chamber.

The details of the configuration and characterization of the devices used in the experiment are given in [7]. In Figure 4.1.2, the setup used to test the programming and homogeneity of the tweezers is drawn. It consists of two laser beams that are both stabilized by measuring their power on a photodiode and using proportional-integral controllers to adjust the signal. The first laser is used for a spin-selecting atoms discussed in the next chapter and has a wavelength of 768 nm. The second laser is the one used for the characterization in [7] and sorting of the atoms, as well as testing everything regarding the tweezers in the following and has a wavelength of 795 nm.

The beams then pass a $\lambda/2$ waveplate to further adjust the polarization, which in turn affects the efficiency of the AOD. The deflector, which is connected to an RF-synthesizer, then produces the 2x2 grid of laser beams. Afterwards, a 75 mm lens, projecting the center of the AOD-array, extends the beam spatially until it is collimated on the 1000 mm lens. This sets the correct beam size in order for the objective to project the beam onto the atoms.

4.2 Sorting algorithms

The ability to change the beam position at will directly leads to being able to rearrange atoms. To do so requires the knowledge about gaps in the pattern, which means when the

atoms are loaded into the initial tweezers, an image is acquired, without destroying the system. From then on, atoms need to move along paths in order to fill the gaps. This has to be done adiabatically, such that no atoms are lost, but also as quickly as possible, since they have a finite, non-negligible, lifetime.

There are some sensible approximation that can be made in order to solve the optimization problem of transporting the atoms with the least amount of moves. For one, we are operating on a rectangular grid and can only move vertically or horizontally and not diagonally. Secondly, atoms that have started moving, are only released when they arrive at their destination. The grid is separated into a target and a reservoir region. While there are still holes in the target region, the algorithm will find a way to fill the gaps using atoms from the reservoir region.

Two algorithms are presented in the following, one is based on solving a pathfinding problem and moves one atom at a time. The other uses the feature of the AOD, that allows to work on a line, trying to move as many atoms as possible at once.

4.2.1 Pathfinding

The pathfinding problem is trying to find the shortest path between two points. For sorting of atoms, this means finding the shortest set of movements to relocate an atom from the reservoir region to an empty spot in the target region. The algorithm in question was developed by Jan Werkmann[1] and is discussed in [8]. One requirement for this implementation is, to reduce the number of 90° turns the atom makes along the path. This results in a simplification that can be made on the algorithm, meaning that an atom moves first along one axis and then the other. This way, there are only two possible paths every atom can take. The optimal path is then the one with the least amount of obstacles in it. Here, an obstacle is simply another atom. If there is one, it segmentizes the path, moving the atom out of the way and the initial atom into its place.

reviewers: is it ok to link the github?

explain in more detail and reference figure

4.2.2 Compression

One advantage of using a digitizer as an RF-synthesizer is the ability to drive the AOD with multiple frequencies at once. This opens the door to moving multiple atoms at the same time. The compression algorithm discussed here makes use of this in order to reduce the

[1] https://github.com/PhyNerd/GridRouting

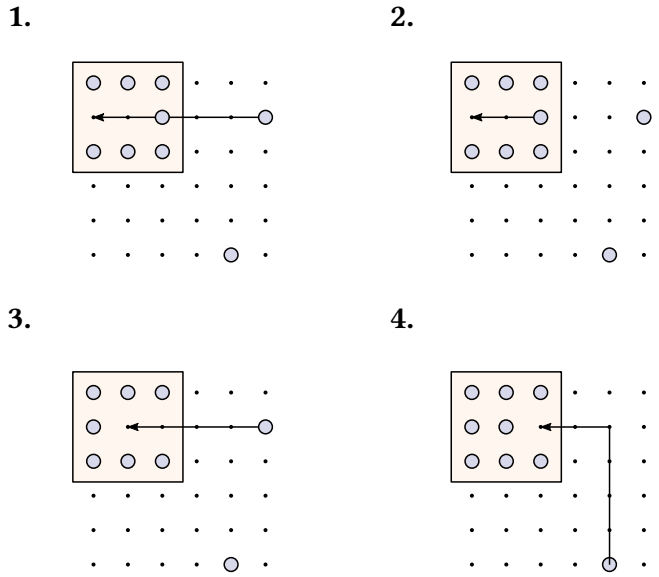

Figure 4.5: Conceptual illustration of the pathfinding algorithm for resorting. The atom tries to move into a hole but is met with an obstacle. The obstacle is first moved out of the way, after which the atom follows. The target area is then further filled with the remaining atom.

total time of the sorting, as well as having a lower computation time with respect to the pathfinding algorithm.

The compression algorithm works by picking a full line of atoms. It then moves the selected atoms along the line towards the target area, grid point by grid point. If an atom would collide with an obstacle, that is, either another atom not currently inside an AOD tweezer, or the end of the target area, then that atom is released and not moved in the next step. This process is how in 4.2.2. When one line is finished moving according to this end condition, the next line is picked up and the process repeated. This is done first for all rows, then for all columns, and finally, all atoms are found in one corner of the grid. Doing it this way, effectively compresses all atoms in the grid into an area.

Due to the nature of the algorithm, there can still be holes in the target area when the sequence is finished. To overcome this problem, the pathfinding algorithm is called at the end of this step, whose runtime is favorable towards low hole numbers.

To further take advantage of the compression algorithm, a geometry is chosen, which has the target area in the center of the grid and the reservoir surrounding it, as seen in Figure . As the algorithm pushes the atoms into a corner, the grid can simply be split up into four sections. Then the moves for each section is individually calculated. Ending up with moves in the row-dimension and moves in the column-dimension for each section, they can then be merged together, if they operate on the same line. As such, the sorting time of moving

fig

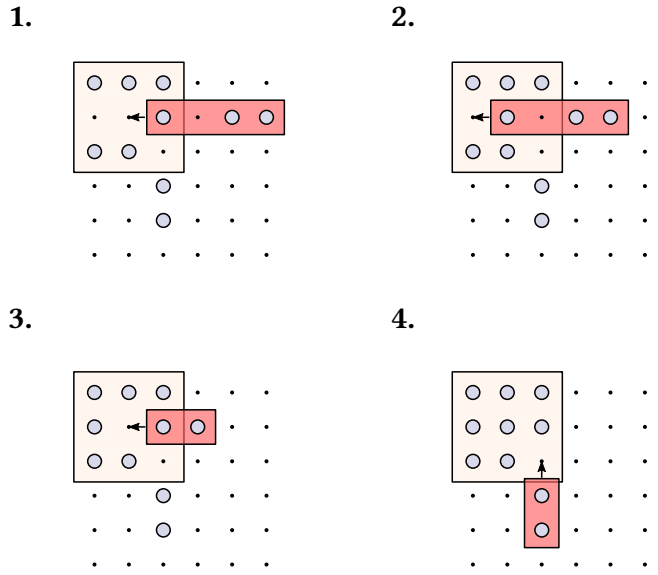

Figure 4.6: Sorting atoms using the compression algorithm is done by selecting a full line of atoms. They are then moved towards the left edge. An atom that meets the edge is released before the others continue moving. When the steps for the rows have are completed, the same process follows for the columns.

atoms into one corner is effectively the same as moving the atoms into the central area, by splitting it up into sections and merging the steps.

4.2.3 Comparison of the two algorithms

As the pathfinding and compression algorithm are both solving the same sorting problem, it is necessary to see a performance comparison between for the two. For this, the target area was chosen to be in the center, surrounded by the reservoir region. This gives a geometry, which has holes as close as possible to reservoir atoms, therefore giving a minimal number of movements for the pathfinding algorithm, while also making use of the performance gain that was highlighted in Section 4.2.2.

Relevant parameters that need to be compared, are the sorting and computation time, as they need to be much slower than the lifetime of the atoms. Atom loss can also occur, whenever the atoms are transferred from the initial tweezer grid to the AOD tweezer grid used for the sorting. This way, the number of transfers are also recorded in the following. Simulations were performed, by populating the full grid with atoms with 50 % probability of occupying a grid point. Then each algorithm was run over this grid and relevant parameters recorded. Simulations were run for various grid sizes, while trying to keep the fraction of number of atoms in the target area N_{target} to the number of atoms in the reservoir area

Pathfinding			
	a_0	a_1	a_2
Resorting time	-3.0×10^{2}	7.2×10^{-1}	3.7×10^{-5}
Computation time	-9.9×10^{-3}	1.5×10^{-5}	9.9×10^{-9}
Number of transfers	-5.8×10^{2}	1.1	7.4×10^{-5}

Compression			
	a_0	a_1	a_2
Resorting time	1.2×10^{1}	2.8×10^{-1}	-1.1×10^{-6}
Computation time	-5.0×10^{-3}	6.8×10^{-6}	8.4×10^{-10}
Number of transfers	5.9×10^{1}	5.5×10^{-1}	-2.4×10^{-6}

Table 4.1: Fit parameters for Figure 4.2.3 by assuming parabola $f(x) = a_0 + a_1 x + a_2 x^2$, x being the atom number.

$N_{reservoir}$ around $\frac{N_{target}}{N_{reservoir}} \approx 0.65$. This has to be compromised for low grid sizes, as the integer nature of grid points only allows natural numbers for reservoir sizes.

The results in Figure 4.2.3 show that the compression algorithm has a faster sorting and computation time, but has to transfer more atoms into the AOD tweezer grid. However, it also shows that it scales better for increasing grid sizes. A polynomial fit is shown for the second half of the points, where the rounding issue is less present. The fit parameters are given in Table 4.2.3, from where it can be seen, that the second order prefactor is negligible. Therefore, from the given data, the algorithms both scale effectively linear to large atom numbers.

4.3 Driving an RF-synthesizer for arbitrary pattern generation

One of the most powerful aspects about AODs is the fact, that a superposition of sound waves results in a superposition of light waves in the output. This way, it is possible to generate a grid of tweezers, by supplying each AOD with one or more RF-frequencies. To synthesize these frequencies, other groups have implemented solutions using phase-locked loops (PLLs) , which can guarantee very stable frequencies. Using these, it is also possible ref

Maximum sampling rate	1.25 GHz
Output level (at max sampling rate)	± 4 V
Transfer speed PC to card	2.8 GB s^{-1}

Table 4.2: Relevant parameters of the Spectrum M4i.6600-x8 card, plugged into a PCIe x8 slot.

to drive frequency ramps, however it is not possible to synthesize multiple frequencies from one PLL. Therefore using this approach it is possible to sort the atoms one-by-one, however it is not possible to generate grid patterns.

To overcome this issue, we implement a digitizer card from Spectrum Instrumentation. Doing so allows to sample arbitrary signals, for example sines, rectangles or even non-periodic ones. A digital-to-analog converter (DAC) on the board converts the sampled points into an analog signal, which can be passed into the AOD.

4.3.1 Functionality of the Spectrum driver

The specific card used in this experiment is the Spectrum M4i.6600-x8 and its specs are summarized in Table 4.3.1. Communication with the card is provided through a low-level interface from the official drivers. In the following is discussed two replay modes of the spectrum card, which are standard replay mode and sequence replay mode. In single replay mode, a signal is sent onto the card, which is played back a set number of times, from start to finish. The sequence replay mode allows to upload sequences during initialization. It is then possible to play any arbitrary combination of the sequences one after another.

The functionality of the card depends on two factors: The layout of the memory, and the readout speed (the sampling rate) of the memory. In the following implementation, two output channels of the spectrum card are used. Doing so, the memory is formatted, such that two bytes of channel 1 data are followed by two bytes of channel 2 data as seen in Figure 4.3.1. Transferring data onto the memory then requires to fill a buffer, that is, memory on the computer running the driver, that has the same layout as the spectrum card's memory.

With this information, the structure of a program driving the digitizer card follows the following format:

In single replay mode:

- Initialization phase
  - Set sampling rate
  - Set replay mode to single replay mode
  - Allocate the buffer memory
- Main loop
  - Sample datapoints of the signal to play and move into the buffer
  - Transfer datapoints from the buffer to the card
  - Replay signal N times.

On the other hand, for the sequence replay mode, the structure is:

- Initialization phase
  - Set sampling rate
  - Set replay mode to sequence replay mode
  - Sample signals to use in the sequence programmed later
  - Transfer signals onto the card
  - Allocate the buffer memory (will contain information about the sequence)
- Main loop
  - Fill buffer with information about which singals to play
  - Transfer buffer to the card
  - Play sequence

The maximum transfer speed for transferring data from the PC to the spectrum card is $2.8\,\mathrm{GB\,s^{-1}}$, this means that it will always be preferrable to move as few data as possible. Consequently, if possible, it is advantageous to use the sequence replay mode, as here, almost all data is already transferred in the initialization phase. All that is left to transfer, is the sequence the data pointer is following.

4.3.2 Limits of using the card in the experiment

There are some considerations to make when using a digitizer card as a driver for acousto-optical tweezers. The first one being, that the transfer of the data onto the card takes time and is given by the sampling rate. This means, that transferring data onto the card while atoms are loaded can be problematic, if the transfer time is on the order of the lifetime of the atoms, since that means that atoms are lost during this time. This can be solved by making use of the sequence replay mode, however to make use of this mode means that a large amount of memory needs to be available on the card.

Variable	Used or assumed value
Sampling rate	1.25 GHz
Central AOD driving frequency	100 MHz
Adiabatic transfer time to new grid	1 ms
Adiabatic movement time to next grid point	1 ms
Grid size	10x10
Number of tweezer transfers for sorting	60
Number of movements for sorting	40

Table 4.3: Variables and assumptions used in the calculations for estimation of data transfer time and memory usage under the consideration of the experiment discussed in this thesis.

In order to calculate the transfer time and memory usage, some assumptions need to be made. The assumptions and all necessary variables are summarized in Table 4.3.2. First of all, the sampling rate is set to be maximal, at $S = 1.25\,\text{GHz}$. This follows, because the central frequency of the AOD is approximately $f_{AOD} = 100\,\text{MHz}$, therefore with the sampling rate above, one period of a sine-signal has at most 13 sampling points. Being able to resolve the signal clearly, has the advantage to generate the frequency more accurately, therefore a good limit is 10 sampling points per period.

Assuming now, that adiabatically transferring an atom from the initial tweezer grid into the AOD tweezer grid takes $t = 1\,\text{ms}$, and moving it one grid space ahead takes the same amount , then the memory M_{sig} one signal occupies is calculated as:

ref

$$n_{points} = St = 1.25 * 10^6 \tag{4.8}$$

$$M_{sig} = 2\,\text{B} * n_{points} = 2.5\,\text{MB}, \tag{4.9}$$

where 1 B is one byte. From the simulations of the algorithms in Figure 4.2.3, we see that assuming a 10x10 grid, there are about 60 tweezer transfers and 40 movements for one sorting. This means 100 sequences need to be played per channel, which is $n_{seq} = 200$ in total. Lastly, the memory for all signals needs to be aligned to a power of two. Therefore, from the transfer speed v_{trf} in Table 4.3.1 follows the time it takes for one transfer t_{trf}:

$$t_{trf} = \text{cpow2}(n_{seq} M_{sig}) v_{trf} = 183\,\text{ms}, \tag{4.10}$$

where the symbol cpow2 refers to rounding up to the next power of two. These calculations set the limit for the single replay mode, however if one decides to use the sequence replay mode, the limiting factor is the memory it takes to store all possible sequences. The storage of the sequences already assumes knowledge of the composition of both channels. Therefore it is necessary to upload every relevant combination of signals for both channels. Working again with a 10x10 grid of atoms, all relevant signals are found from the following table:

Signals on channel 1	Signals on channel 2	Usage
10 intensity ramps up	10 intensity ramps up	Transfer into AOD grid
10 intensity ramps down	10 intensity ramps down	Transfer out of AOD grid
9 frequency ramps up	10 constant frequencies	Move along x-axis
9 frequency ramps down	10 constant frequencies	Move along x-axis
10 constant frequencies	9 frequency ramps up	Move along y-axis
10 constant frequencies	9 frequency ramps down	Move along y-axis

Therefore there are 560 combinations and $n_{seq} = 560 * 2 = 1120$ signals to upload onto the card. Each having a size of $M_{sig} = 2.5\,\text{MB}$ results in a required memory of $M_{req} = 2.8\,\text{GB}$. More generally, on a NxM grid, the number of sequences can be calculated via

$$n_{seq} = 2NM + 2N(M-1) + 2(N-1)M \tag{4.11}$$

and therefore the required memory is

$$M_{req} = 5\,\text{MB} n_{seq}. \tag{4.12}$$

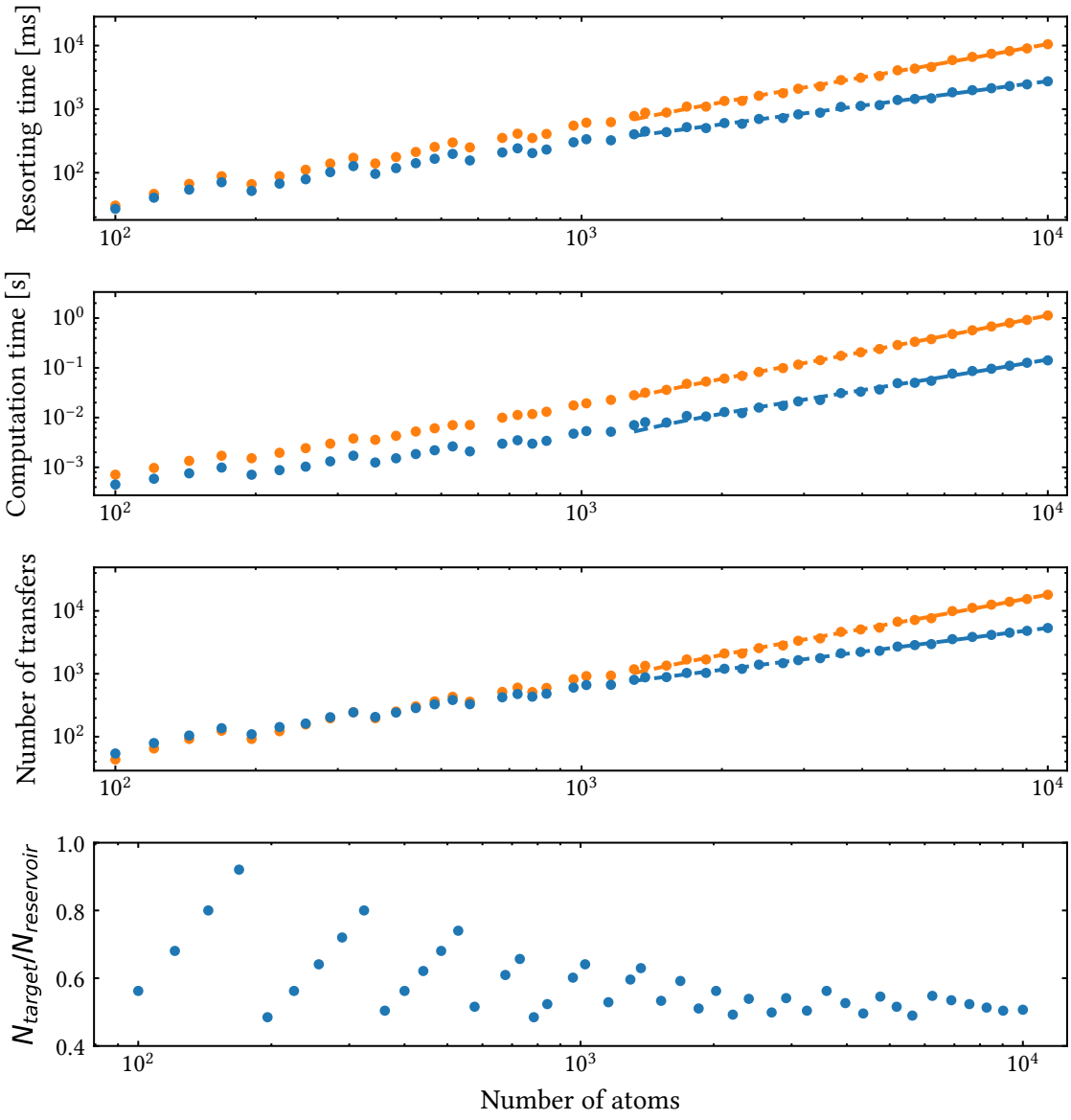

Figure 4.7: Comparison of pathfinding algorithm (orange) and compression algorithm (blue) for sorting atoms into a target region. For each data point, 50 simulations were run and the mean of the result is shown. Standard deviation is on the size of the dots drawn and as as such are not visible. The fraction of atoms in the target versus the reservoir area are shown in the last diagram. Since only integer values are allowed for the reservoir size, the fraction between the two sees a rounding effect. For this reason, the fit is only done for the upper half of the data points, where the effect is less pronounced. The values to the fit are given in Table 4.2.3.

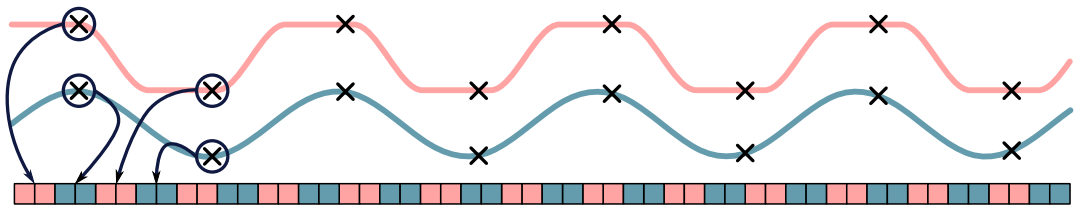

Figure 4.8: Sampled data points are stored in a local buffer, which can then be transferred into the cards memory. The memory is effectively 1-dimensional, with two bytes for each sampled data point. Example signals are given for Channel 1 (red) and Channel 2 (blue). In the single replay mode, the data pointer will read from the first memory position until a given end point. In sequence replay mode, the data pointer will move forward, but can jump at any point based on user preference.

5 Spin-selective imaging

5.1 Approaches

5.1.1 Zeemann induced potential separation

5.1.2 Utilization of magic wavelengths

5.2 Setup

5.2.1 Schematics

5.2.2 Cavity classification

6 Conclusion

Bibliography

1. Duda, M. *A Laser System for Cooling and Trapping Potassium-39, Msc-thesis* tech. rep. (2017) (cit. on pp. 5, 15) .
2. Saleh, B. E. A. & Teich, M. C. *Fundamentals of Photonics* (John Wiley & Sons, Inc., New York, USA, Aug. 1991) (cit. on pp. 7, 16) .
3. BME Bergmann. *Pockels Cell Driver Head* `https://web.archive.org/web/20200712183516/https://www.bme-bergmann.de/high-voltage-electronics/pockels-cell-driver-head/` (09/14/2020) (cit. on p. 11) .
4. Cooper, A. *et al.* Alkaline-Earth Atoms in Optical Tweezers. *Physical Review X* **8** (Dec. 2018) (cit. on p. 15) .
5. Barredo, D., De Léséleuc, S., Lienhard, V., Lahaye, T. & Browaeys, A. An atom-by-atom assembler of defect-free arbitrary two-dimensional atomic arrays. *Science* **354,** 1021–1023 (Nov. 2016) (cit. on p. 15) .
6. Endres, M. *et al.* Atom-by-atom assembly of defect-free one-dimensional cold atom arrays. *Science* **354,** 1024–1027 (Nov. 2016) (cit. on p. 15) .
7. Osterholz, P. *Freely Configurable Holographic Trap Arrays for the Trapping of Single Atoms, Msc-thesis* tech. rep. (2020) (cit. on p. 19) .
8. Ohl de Mello, D., Birkl, G. & Walther, T. Rydberg interactions in a defect-free array of single-atom quantum systems (2020) (cit. on p. 20) .

Statement of Authorship

I herewith declare that this thesis was solely composed by myself and that it constitutes my own work unless otherwise acknowledged in the text. I confirm that any quotes, arguments or concepts developed by another author and all sources of information are referenced throughout the thesis. This work has not been accepted in any previous application for a degree.

Munich, October 16, 2020

Signature